

Assembly and Test of HD2, a 36 mm bore high field Nb₃Sn Dipole Magnet

P. Ferracin, B. Bingham, S. Caspi, D. W. Cheng, D. R. Dietderich, H. Felice, A. Godeke, A. R. Hafalia, C. R. Hannaford, J. Joseph, A. F. Lietzke, J. Lizarazo, G. Sabbi, F. Trillaud, and X. Wang

Abstract—We report on the fabrication, assembly, and test of the Nb₃Sn dipole magnet HD2. The magnet, aimed at demonstrating the application of Nb₃Sn superconductor in high field accelerator-type dipoles, features a 36 mm clear bore surrounded by block-type coils with tilted ends. The coil design is optimized to minimize geometric harmonics in the aperture and the magnetic peak field on the conductor in the coil ends. The target bore field of 15 T at 4.3 K is consistent with critical current measurements of extracted strands. The coils are horizontally pre-stressed during assembly using an external aluminum shell pre-tensioned with water-pressurized bladders. Axial pre-loading of the coil ends is accomplished through two end plates and four aluminum tension rods. The strain in coil, shell, and rods is monitored with strain gauges during assembly, cool-down and magnet excitation, and compared with 3D finite element computations. Magnet's training performance, quench locations, and ramp-rate dependence are then analyzed and discussed.

Index Terms—Dipole magnet, Nb₃Sn

I. INTRODUCTION

THE LBNL Superconducting Magnet Program, as part of the development of Nb₃Sn high field magnets for the next generation of HEP colliders [1], has fabricated and tested the Nb₃Sn dipole magnet HD2 (see Fig. 1). After a preliminary description of the conceptual design reported in [2], we presented the results of a detailed mechanical analysis of coil and structure in [3], and documented the final design, the fabrication and assembly procedure, as well as the field quality expectations, in [4]. In this paper, the results of three tests carried out at the LBNL test facility are presented, including strain gauges measurements, training performance, quench locations, and ramp-rate studies.

II. MAGNET DESIGN

The HD2 magnet design (Fig. 2) features two block-type coils wound around a Ti alloy pole with a cut-out for a 36 mm aperture bore tube. The coil has a straight section of 475 mm and in the ends tilts up at a 10° angle through hard-way bends.

Manuscript received 19 August 2008. This work was supported by the Director, Office of Energy Research, Office of High Energy and Nuclear Physics, High Energy Physics Division, U. S. Department of Energy, under Contract No. DE-AC02-05CH11231.

All authors are with Lawrence Berkeley National Lab, Berkeley, CA 94720 USA (phone: 510-486-4630; fax: 510-486-5310; e-mail: pferracin@lbl.gov).

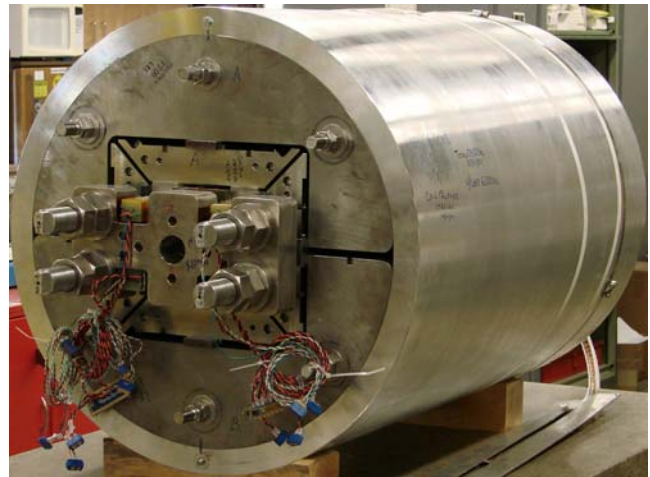


Fig. 1. HD2 assembled and pre-loaded.

The peak field is located in the straight section of layer 2 pole turn: layer 1 pole turn and the coil ends have a field margin of respectively 4% and 6%. The yoke cross-section has been designed to have, in the current range of 2-17 kA, a Δb_3 of ± 1.3 units and a Δb_5 of ± 0.1 units at a $R_{ref} = 10$ mm. The geometric harmonics, optimized for a current of 16 kA, are within 0.1 units. The support structure is based on a 41 mm thick Al shell pre-tensioned with water-pressurized bladders. With a pre-load level for a 15 T bore field, the coil reaches a peak compressive stress of -180 MPa in the layer 1 pole turn.

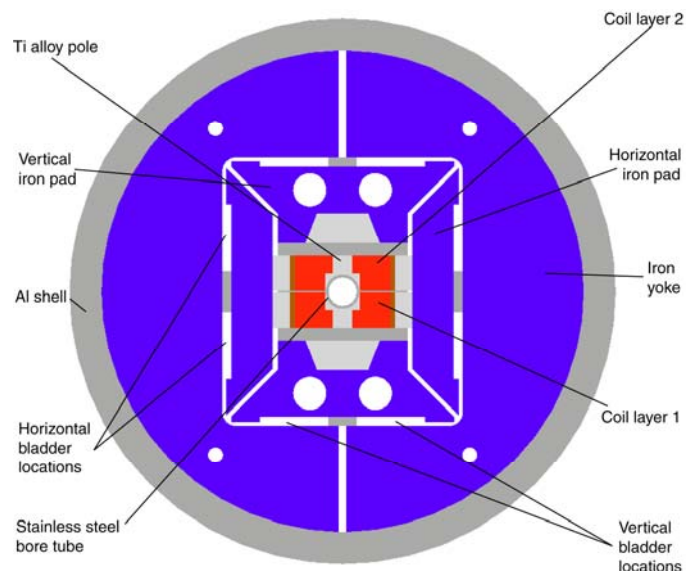


Fig. 2. HD2 cross-section.

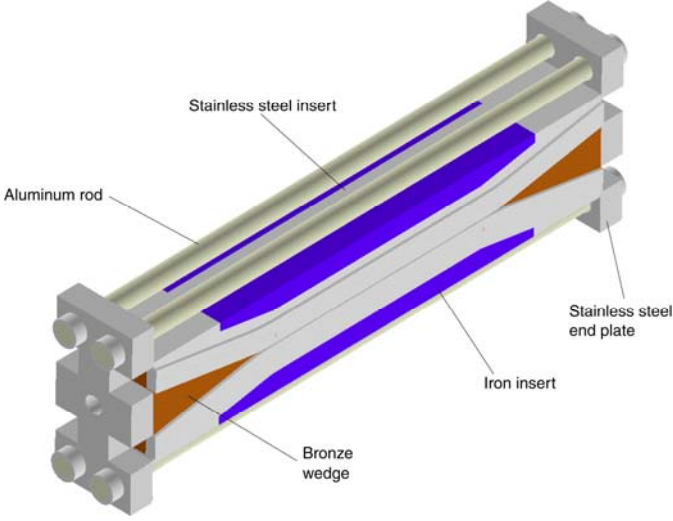


Fig. 3. HD2 coil end support.

Two 50 mm thick endplates, connected by four 18.5 mm diameter Al rods, support the coil ends (see Fig. 3).

III. CONDUCTOR AND MAGNET PARAMETERS

Three coils, composed of two layers wound from a continuous length of cable made of 51 RRP strands with a 0.8 mm diameter, were fabricated and tested. The strand and cable parameters are listed in Table I. Both virgin (round) strands and strands extracted from cables were reacted with the coils to analyze magnet performance. In Fig 4 the critical current measurements are plotted as a function of the total magnetic fields, both for virgin and extracted strands used for coil 2 and 3. A self-field correction of 0.4858 T/kA is included. Data are fitted and extrapolated at different temperatures using the ITER standard parameterization [5]. At 12 T and 4.2 K, the strands exhibit a critical current cabling degradation of 4% in coil 1 and 2% in coil 2 and 3.

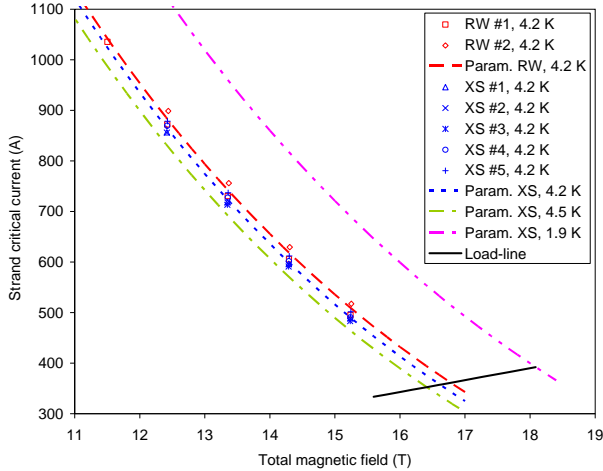


Fig. 4. Critical current (A) vs. total magnetic field (T) measurements and parameterization curves of round (RW) and extracted wires (XS) for coil 2-3.

The intersection of the magnet load-line and the 4.3 K (magnet test temperature) parameterization curve provide an expected magnet current limit (short sample current I_{ss}) at 4.3 K of 17.3 kA or 18.1 kA, assuming respectively coil 1 or coil 2 and 3 properties (see Table II for all magnet parameters). At 1.9 K, an increase of 1.5 T is expected in maximum bore field.

TABLE I CABLE PARAMETERS

Parameter	Unit	Coil 1	Coil 2-3
Strand diameter (before reaction)	mm	0.802	0.801
Process		Restacked Rod Process	
Stack		54/61	
Non Cu %		51	54
RRR		16	287
Twist pitch	mm	13	14
No. strands		51	
Cable width (bare)	mm	22.008	21.999
Cable thickness (bare)	mm	1.401	1.406
Insulation thickness	mm	0.095	

TABLE II MAGNET PARAMETERS

Parameter	Unit	HD2a-b	HD2c
Clear aperture	mm	36	
Magnet outer diameter	mm	705	
No. turns in layer 1 (quadrant)		24	
No. turns in layer 2 (quadrant)		30	
Short sample current I_{ss} at 4.3/1.9 K	kA	17.3/19.2	18.1/20.0
Bore field at 4.3/1.9 K I_{ss}	T	15.0/16.5	15.6/17.1
Coil peak field at 4.3/1.9 K I_{ss}	T	15.9/17.4	16.5/18.1
Fx/Fy layer 1 (quadrant) at 17.3 kA	MN/m	+2.3/-0.4	
Fz layer 1 (quadrant) at 17.3 kA	kN	90	
Fx /Fy layer 2 (quadrant) at 17.3 kA	MN/m	+3.3/-2.2	
Fz layer 2 (quadrant) at 17.3 kA	kN	126	
Stored energy at 17.3 kA	MJ/m	0.84	
Inductance	mH/m	5.6	

HD2a and HD2b were assembled with coil 1 and coil 2. HD2c was assembled with coil 2 and coil 3.

IV. ASSEMBLY AND TEST OVERVIEW

HD2 underwent three tests at 4.3 K: HD2a and HD2b with coil 1 and coil 2, and HD2c with coil 2 and coil 3. The shell and the aluminum rods were instrumented with strain gauges, and their stress conditions were monitored and recorded during all room-temperature loadings, cool-downs, and tests. Fig. 5 and Fig. 6 show the evolution of the shell and rod stress, with a comparison with the expectations from a 3D finite element model of the entire magnet assembly [2].

In order to mechanically characterize the structure and validate the numerical model, a first cool-down to LN temperature was performed. Coil 1 and coil 2 were assembled and pre-loaded inside the structure. During cool-down, the tension increased from 49 MPa to 135 MPa in the shell and from 34 MPa to 83 MPa in the rods.

Since the data were considered consistent with model expectations, after warm-up the magnet was cooled-down to 4.3 K, without disassembly or change in pre-load, and tested (HD2a). At 4.3 K the measured shell stress was 144 MPa, while a total axial force of 560 kN was provided to the coil ends by the rods tensioned to 90 MPa. According to the model, this stress conditions in the structure results in a coil peak stress in the straight section of -149 MPa and ensures no separation coil-pole, both in the straight section and in the end region, up to a 14 T bore field.

HD2b test was carried out after a minor adjustment of the coil end support, without unloading the shell.

The last tests (HD2c) followed a complete disassembly where coil 1 was replaced by coil 3 and the shell tension was increased by 13 MPa at 293 K, from 36 MPa to 49 MPa.

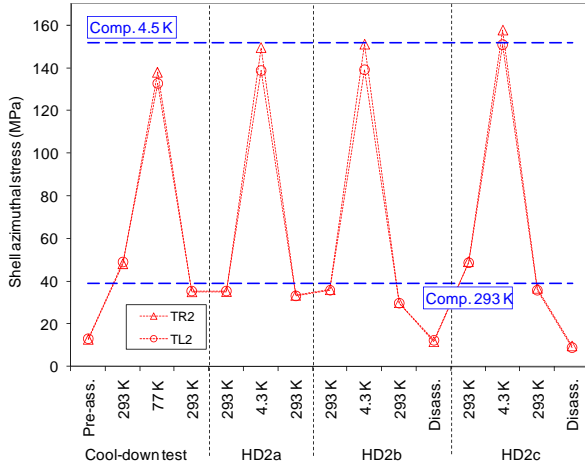


Fig. 5. Azimuthal stress (MPa) of the 41 mm thick aluminum shell during pre-load and tests: measured values (markers) and model expectations (dashed lines).

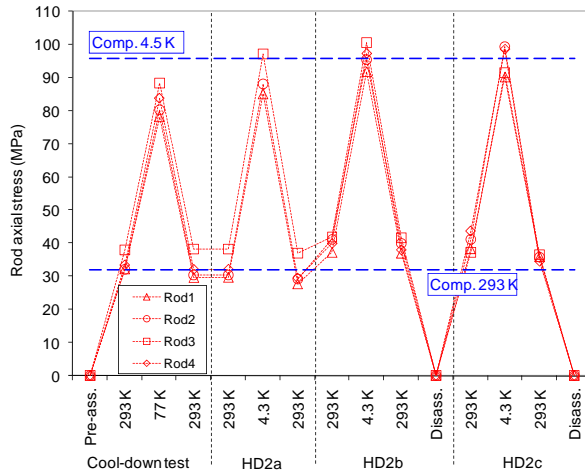


Fig. 6. Axial stress (MPa) of the four 18.5 mm diameter rods during pre-load and tests: measured values (markers) and model expectations (dashed lines).

V. TEST RESULTS

A. Training Quenches

The training histories of the three tests are shown in Fig. 7, where the bore field is plotted for all the low ramp-rate quenches. The bore field was measured with a Hall probe placed in the longitudinal center of the magnet (see Fig. 8 for a measured and computed bore field vs. current).

HD2a had a first quench at a bore field of 11.4 T (73% of I_{ss}). After 16 quenches it reached a maximum bore field of 13.3 T (87% of I_{ss}), corresponding to an estimated coil peak field of 14.0 T. In the second test (HD2b), the magnet did not exhibit memory of the previous quench performance, and, after a first quench at 11.0 T (71% of I_{ss}), it trained to the same maximum field after 12 quenches.

Because of a failure of the extraction system during quench #12, the number of MIITS released to coil 1 (quenching coil) increased from 16 to 23. As a result, higher ramp-rate sensitivity was observed, and a reduction of the ramp-rate from 20 to 10 A/s was required to achieve the previous level of bore field (quenches #15 and #16). A detailed comparison of the voltage signals recorded before and after training quench #12 is presented in [6].

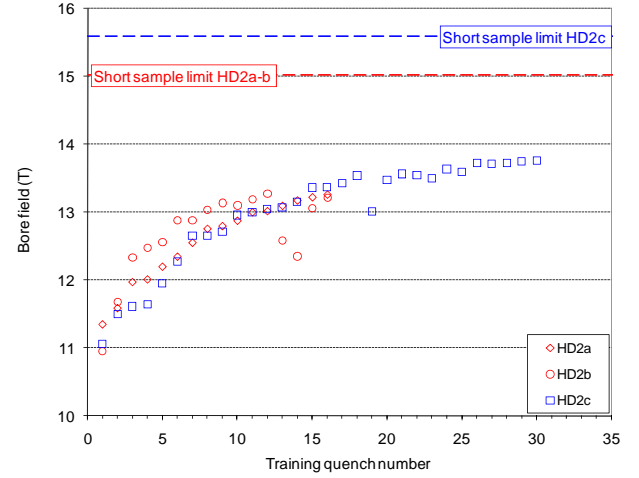


Fig. 7. Training quenches in HD2a, HD2b, and HD2c. The short limit of 15.0 (15.6) T bore field corresponds to a coil peak field of 15.9 (16.5) T. All the plotted quenches occurred at a current ramp rate ≤ 20 A/s.

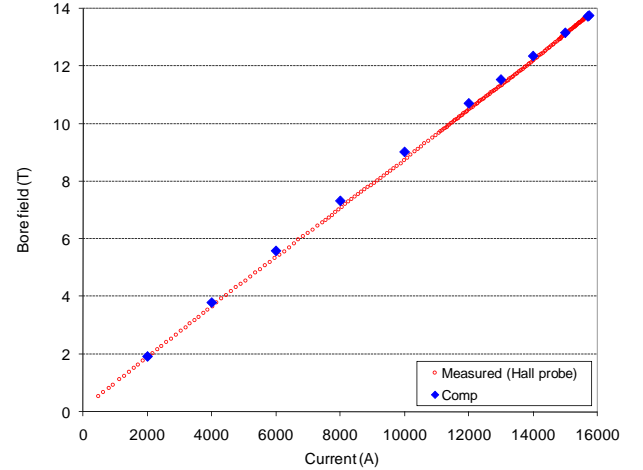


Fig. 8. Measured and computed bore field (T) vs. magnet current (A).

After a 13 MPa increase of shell tension and the replacement of coil 1 with coil 3, the magnet was retested as HD2c. Despite an increase of the expected short sample limit (see Table II), the training was similar as in the previous tests; the magnet, at a ramp rate of 5 A/s, reached a maximum bore field of 13.8 T (87% of I_{ss}) at quench #30, corresponding to an estimated peak field of 14.5 T.

B. Quench Locations

The time-of-flight method was used to locate the quench origins. The voltage signals were monitored using derivative amplifier with a resolution of 5 kHz. Normal zone propagation velocity was determined based on the correlation between I_q/I_{ss} and the velocity v given by $v = a \cdot \exp(b \cdot I_q/I_{ss})$, where $a = 0.590$, $b = 4.554$, I_q is the quench current, and I_{ss} is the current limit of the quenching segment. The correlation was obtained from test results of the SQ02 magnet [7]. Equal and constant velocities of both normal fronts were assumed. In Fig. 9-11, the quench origins in HD2a, HD2b and HD2c are plotted. The inner and outer loops represent respectively the pole turn of layer 2 and layer 1, while the vertical dashed lines indicate the end of the straight section, approximately where the cable hard-way bend starts. For each magnet test, the origins are projected to a plane parallel to the coil mid-plane.

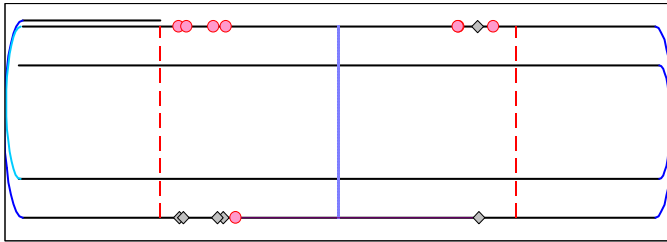


Fig. 9. HD2a quench locations: coil 1 (diamond markers) and coil 2 (round markers).

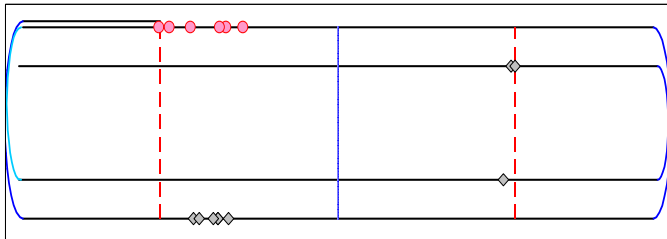


Fig. 10. HD2b quench locations: coil 1 (diamond markers) and coil 2 (round markers).

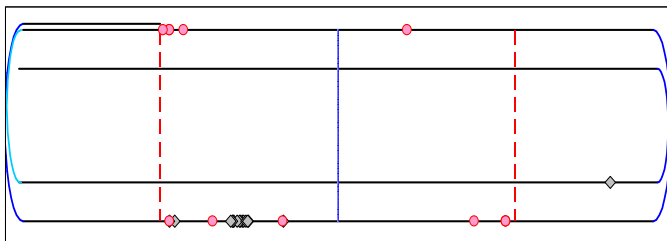


Fig. 11. HD2c quench locations: coil 3 (diamond markers) and coil 2 (round markers).

The voltage signals recorded during the HD2a test allowed determining the position of 14 training quenches out of 16 (see Fig. 9). The quenches were almost evenly distributed between the coils: 6 in coil 1 and 8 in coil 2 (which featured a higher expected short sample current). They all occurred in the pole turn of layer 1, which has a 4% margin in field with respect to the pole turn in layer 2. In addition, they were all located towards the end of the straight section, close to the region where the conductors are hard-way bent.

All the training quench locations of HD2b were identified but one (see Fig. 10). Before quench #12, 4(6) quenches occurred in coil 1(2), confirming that the lower current limit of coil 1 was not affecting the magnet training. After quench #12, the remaining four quenches took place all in coil 1 (indicating a possible conductor damage). Most of the quenches (12) were again located towards the end of the straight section of layer 1 pole turn, while three occurred in the pole turn of layer 2 in coil 1 (peak field region).

In the HD2c test, coil 1 was replaced by coil 3. Out of 30 training quenches, 28 positions were determined (see Fig. 11). All but one were again located in the pole turn of layer 1. Most of the 16 quenches occurred in coil 3 were concentrated at a single location 90 mm from the ramp towards to center of the coil. The 12 quenches in coil 2 spread in the straight sections of both the lead and return side. It was also recorded that, for 11 times during training, quenches occurred simultaneously (within 1 ms) in both coils and in adjacent locations (pole turn, layer 1, similar longitudinal location, same coil side), indicating that quenches started at the mid-plane in between the two coils.

C. Ramp-rate dependence study

Ramp-rate dependence studies were performed during the HD2c test. Ramp-rate was varied from 5 A/s to 300 A/s. In Fig. 12, we plot the ratio of the highest quench current with respect to I_{ss} as a function of ramp-rate. High ramp-rate quenches were originated both before and after magnet training: no degradation was observed.

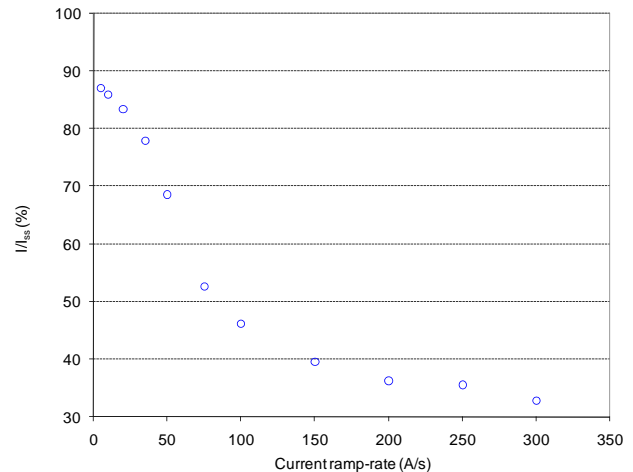


Fig. 12. Ratio of quench current with respect to I_{ss} as a function of ramp-rate

VI. CONCLUSIONS

The Nb₃Sn dipole magnet HD2 was assembled, loaded, and tested three times at 4.3 K at LBNL. The coil design includes a clear aperture of 36 mm and has been optimized to minimize geometric harmonics. The magnet reached a maximum bore field of 13.8 T (87% of I_{ss}), corresponding to an estimated peak field on the conductor of 14.5 T. The quenches were almost evenly distributed among the coils, despite of differences in conductor properties. In addition, they were mostly located at the end of the straight section of the layer 1 pole turn, where the field is about 4% lower than in layer 2. At the moment, the quench performance seems to point at a possible lack of mechanical support in the mid-plane area close to the coil hard-way bend. Further tests are considered in the coming months to perform field quality measurements, to increase the clear aperture, and to optimize coil pre-load.

REFERENCES

- [1] A. F. Lietzke, *et al.*, "Test results for HD1, a 16 Tesla Nb₃Sn dipole magnet", *IEEE Trans. Appl. Supercond.*, vol. 14, no. 2, June 2004, pp. 345-348.
- [2] G. Sabbi, *et al.*, "Design of HD2: a 15 T Nb₃Sn dipole with a 35 mm bore", *IEEE Trans. Appl. Supercond.*, vol. 15, no. 2, June 2005, pp. 1128-1131.
- [3] P. Ferracin, *et al.*, "Mechanical design of HD2, a 15 T Nb₃Sn dipole magnet with a 35 mm bore", *IEEE Trans. Appl. Supercond.*, vol. 16, no. 2, June 2006, pp. 378-381.
- [4] P. Ferracin, *et al.*, "Development of the 15 T Nb₃Sn Dipole HD2", *IEEE Trans. Appl. Supercond.*, vol. 18, no. 2, June 2008, pp. 277-280.
- [5] A. Godeke, B. ten Haken, H. H. J. ten Kate, and D. C. Larbalestier, "A general scaling relation for the critical current density in Nb₃Sn", *Supercond. Sci. Technol.*, vol. 19, 2006, pp. R100-R116.
- [6] J. Lizarazo, *et al.*, "Use of High Resolution DAQ System to Aid Diagnosis of HD2b, a High Field Nb₃Sn Dipole", presented at *2008 Applied Superconductivity Conference*, Chicago, IL, USA, August 17-22, 2008.
- [7] P. Ferracin, *et al.*, "Assembly and Tests of SQ02, a Nb₃Sn Racetrack Quadrupole Magnet for LARP", *IEEE Trans. Appl. Supercond.*, vol. 17, no. 2, June 2007, pp. 1019-1022.